AN 8mm SOLID STATE SPECTROMETER

by

KER PING LEE

B.Sc., Chung Chi College, 1960

A THESIS SUBMITTED IN PARTIAL FULFILMENT OF

THE REQUIREMENTS FOR THE DEGREE OF

MASTER OF SCIENCE

in the Department

of

PHYSICS

We accept this thesis as conforming to the

required standard

THE UNIVERSITY OF BRITISH COLUMBIA

December, 1962

In presenting this thesis in partial fulfilment of

the requirements for an advanced degree at the University of

British Columbia, I agree that the Library shall make it freely

available for reference and study. I further agree that permission

for extensive copying of this thesis for scholarly purposes may be

granted by the Head of my Department or by his representatives.

It is understood that copying or publication of this thesis for

financial gain shall not be allowed without my written permission.

Department of _Physics_

The University of British Columbia,
Vancouver 8, Canada.

Date _14 Jan. 1963._

ABSTRACT

A sensitive, wide or narrow band, solid state spectrometer

operating at a wavelength of 0.85 cm has been built which is

described in detail. The spectrometer is of the crystal detector

reflection-cavity-in-magic-Tee-bridge type and can operate from

room down to liquid helium temperatures. The cavity is excited in

the TE_{111} mode and the magnetic field modulated at 140 cps. Both

large and small field modulations are incorporated for scope

presentation of linewidth varying from about 0.5 to 500 gauss.

Signals from single crystals of copper sulphate pentahydrate and

polycrystalline 1-1-diphenyl-2-picryl hydrazyl (DPPH) have been

obtained. From the latter, a sensitivity limit of about 10^{-8} gram

is obtained at room temperature for a bandwidth of 1 cps indicating

a sensitivity of the order of 10^{-11} gram at 4.2° K. Various methods

of improvement were discussed in order to reach the ultimate

sensitivity.

ACKNOWLEDGMENT

TABLE OF CONTENTS

LIST OF TABLES

LIST OF ILLUSTRATIONS

LIST OF PLATES

CHAPTER I

INTRODUCTION

Magnetic resonance is a branch of radio-frequency spectroscopy invaluable to the study of the solid state. It can be classified into nuclear, ferromagnetic, antiferromagnetic and paramagnetic resonance. Nuclear resonance is concerned with nuclear dipoles, the others with electronic dipoles. In ferromagnetic and antiferromagnetic substances, the electronic dipoles are strongly coupled together by exchange forces while in paramagnetic materials, the electronic dipoles form a loosely coupled system; each paramagnetic ion may be treated individually.

The phenomenon of paramagnetism occurs whenever a system of charges has a resultant angular momentum. If this momentum is of electronic origin, one speaks of electronic paramagnetism. For instance, paramagnetism can be found in atoms and molecules having an odd number of electrons, in molecules with an even number of electrons but having a resultant angular momentum, in the so-called colour centres, in metals and semiconductors (caused by conduction electrons).

The properties of the paramagnetic ion can be obtained from measurements of the susceptibility, specific heat, gyromagnetic ratio, Faraday effect, paramagnetic relaxation and paramagnetic resonance. However only the last method enables studies to be made from the microscopic

point of view. It is also more sensitive than any of the other methods. Consequently, it can deal with very small quantities of paramagnetic substance. This is very convenient and often advantageous.

A considerable amount of research has been carried out on microwave absorption in solid state compounds and most attention has been given to paramagnetic resonance absorption. The results obtained from an analysis of these spectra give considerable information on forces and interactions existing in the solid state. Paramagnetic resonance gives the most direct and accurate description of the ground state and of the effect of crystalline field on the energy levels of the paramagnetic ion. Its high sensitivity also permits the perturbations of the nuclear spin and nuclear electric quadrupole moment to be detected.

In this thesis, we shall be concerned with the design of a spectrometer suitable for such studies. A short account of the theory of paramagnetic resonance will be given in Chapter II. Chapters III and IV give the descriptions of the apparatus and the experimental procedure in detail. Following are the experimental results obtained from the testing of the spectrometer.

CHAPTER II

QUANTUM THEORY OF PARAMAGNETISM

Excellent summaries of the experimental and theoretical aspects of paramagnetic resonance can be found in the review article by Bleaney and Stevens (B4) and in a complementary review by Bowers and Owen (B5). In this chapter, the theory will be briefly discussed. For more detail, the reader is referred to the above-mentioned articles together with the texts by Low (L2) and Ingram (I1).

2.1 The Magnetic Resonance Phenomenon

2.1.1 Resonance Condition

If a free ion of a resultant angular momentum J is placed in a uniform magnetic field H, the energy levels corresponding to the various spatial orientation of J are given by

$$W = g \beta HM \tag{2.1}$$

g is the Landé g factor and $\beta = \dfrac{eh}{4\pi mc}$ is the Bohr magneton; e, m are the charge and mass of the electron, c is the velocity of light, h is Planck's constant, M is the component of J along the field acting on the ion. If an alternating field of frequency ν is applied at right

angles to H, magnetic dipole transitions are produced when

$$h\nu = g\beta H \qquad\qquad (2.2)$$

according to the selection rule $\Delta M = \pm 1$.

In a system of ions in thermal equilibrium with their surroundings, the lowest state has the greatest population. Since transitions up and down have the same a priori probability, the net result is a greater absorption than emission of energy causing a damping of the tuned circuit with which the paramagnetic substance is coupled.

2.1.2 Fine Structure

The degeneracy of the ground state of a paramagnetic ion in a crystal is often lifted by the crystalline electric field and other interactions. Consider an ion of spin 3/2 with an initial splitting between the doublets $M_S = \pm \frac{1}{2}$ and $M_S = \pm 3/2$ due to an axial crystalline field (Fig. 1). The energy levels diverge linearly when a magnetic field is applied along the axis which is taken as the axis of quantization. An oscillating magnetic field component perpendicular to the axis induces transitions $\Delta M_S = \pm 1$ and the parallel component induces transitions $\Delta M_S = 0$. In $\Delta M_S = \pm 1$ transitions, a triplet structure results when the frequency is kept constant as indicated by the arrows in Fig. 1 and the magnetic field is varied. This forms the 'fine structure' of the spectrum.

In Cu^{2+} ion shown in Fig. 2 (I1), most of the total degeneracy of $(2L+1)(2S+1) = 10$ is removed by the cubic and tetragonal fields of the

M_s

$+3/2$

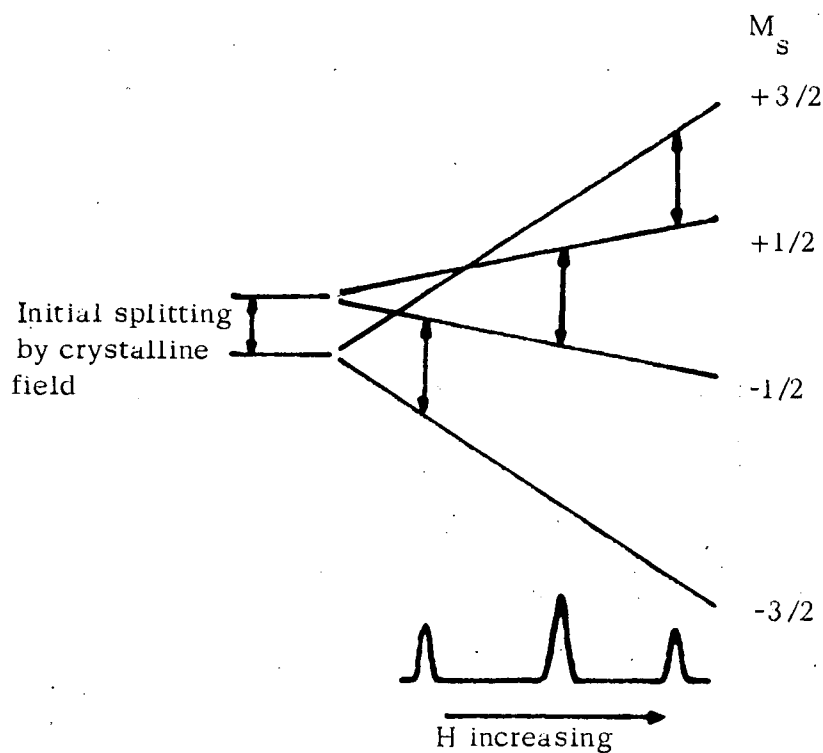$+1/2$

Initial splitting
by crystalline
field

$-1/2$

$-3/2$

H increasing

Fig. 1 Energy Level Diagram for S=3/2 ion with Magnetic Field
H Parallel to the Axis of the Crystalline Field.

Ground State ^{2}D

E_1

$h\nu = g\beta H$

Free Ion	Cubic Field	Tetragonal Field	Spin-orbit Coupling	Magnetic Field

Fig.2 Electron Splittings of Cu^{+2}

crystalline lattice, the whole of the degeneracy being removed by the addition of the spin-orbit interaction. According to Kramers theorem (K2) an ion having an odd number of electrons must have its energy levels remain two-fold degenerate and the degeneracy can be raised only by an applied magnetic field. Since the orbital splittings are very large all the copper ions will be in the lowest state E_1, and we have a paramagnetic resonance absorption spectrum without fine structure.

2.1.3. Hyperfine Structure

When the nucleus of a paramagnetic ion also possesses a resultant angular momentum I and hence a magnetic moment, there will be an interaction with the electronic motion. In a strong external magnetic field, each electronic level is split into (2I+1) levels due to the (2I+1) different orientations of the nucleus. The oscillating field exerts a negligible effect on the nuclear moment (about 10^3 times smaller than that of the electron) so that the allowed transitions become $\Delta M_I = 0$. This together with $\Delta M_S = \pm 1$ selection rule gives (2I+1) hyperfine lines. Since at normal temperatures all nuclear orientations are equally probable, the lines will have equal intensity. Also in a strong field, the energy levels vary linearly with the field. The lines are therefore equally spaced. If the external field is comparable to that produced by the nucleus, the component hyperfine levels will contain an admixture of different M_I states giving rise to unequal splitting of the levels. When two states contain the same value of M_I, a transition is allowed which appears to be "forbidden" when the states are labelled by their strong field quantum numbers.

Another cause of unequal spacing is due to the interaction of the nuclear electric quadrupole moment with the gradient of the electric field produced at the nucleus. If the applied field is parallel to the gradient of the electric field, this interaction will shift the energy levels by an amount proportional to M_I^2. If the two directions are not parallel, the various nuclear states are admixed and forbidden transitions result as before.

2.2 Theory of Line Width

Very often, the resolution of the fine structure and hyperfine structure is limited, not by instrumental effects, but by the line widths of the absorption lines. This width is dependent upon the interaction between the paramagnetic ions and their surroundings and on the interaction among the ions themselves. The natural line width arises from the finite lifetime of a given state and is completely negligible compared with the other factors (I1). It will not be discussed here. The other more important sources of broadening will be briefly treated below.

2.2.1 Spin-Lattice Interaction

The spin-lattice interaction may be characterized by a spin-lattice relaxation time T_1 which is a measure of the rate at which a spin system approaches equilibrium with the lattice after having been disturbed by the absorption of energy. The mechanisms have been discussed by many authors (L2).

There is the indirect process or Raman process in which the spins

transfer energy with the lattice by means of inelastic scattering of phonons. For the case of $S = 1/2$, $T_1 \propto \Delta^6/\lambda^2 T^7$ for $T <$ Debye temperature Θ_D and proportional to T^{-2} for $T > \Theta_D$. Δ is the height of the next orbital above the ground state and λ is the spin-orbit coupling coefficient.

If the spins exchange a quantum of energy directly with a lattice vibration of the appropriate frequency, we have the direct process. Then $T_1 \propto H^{-2}T^{-1}$ for non-Kramers salts (even number of electrons) and $T_1 \propto H^{-4}T^{-1}$ for Kramers salts. The Orbach process (O1), arising from phonon resonance effects, gives $T_1 \propto \exp(\Delta/kT)$.

Spin-lattice relaxation is the predominant line broadening mechanism at high temperatures. In practice the temperature at which measurements are made is always reduced until the line width is due to spin-spin rather than spin-lattice interaction.

2.2.2 Spin-Spin Interaction

The second broadening effect arises from the interaction between the dipoles which can be regarded as rather like bar magnets precessing about the external field. The component in the field direction sets up a steady field at the neighbours altering the total field value slightly. This process of broadening is similar to that produced by an inhomogeneous magnetic field. Also the rotating component sets up a rotating field which may induce transitions in the neighbouring ions and thus decreasing the normal lifetime of the energy state. A broadening results as a consequence of the Uncertainty Principle.

The theory of spin-spin interaction has been developed by

Van Vleck (V2) and Pryce and Stevens (P4). For free spins, the mean-square width as given by Van Vleck is

$$(\Delta H)^2 = \frac{3}{4} S(S+1)g^2 \beta^2 \sum_k \left\{ \frac{1-3\cos^2\theta}{r^3} \right\}_{jk}^2$$

$$+ \frac{1}{3} S'(S'+1) \frac{g'^4}{g^2} \beta^2 \sum_{k'} \left\{ \frac{1-3\cos^2\theta}{r^3} \right\}_{jk}^2 \qquad (2.3)$$

where θ is the angle between the lines joining the dipoles and the direction of the applied field

r being the distance between the j and kth ion.

The second term refers to interaction between dissimilar ions.

This dipolar interaction can also be described by a relaxation time T_2 as defined by

$$T_2 = \frac{1}{2} \left[g(\nu) \right]_{max} \qquad (2.4)$$

where $g(\nu)$ is the normalised line shape function.

2.2.3 Exchange Interaction

If the paramagnetic ions are close enough together exchange inter-action may occur between them, which can alter the line width consider-ably. When the spins are identical and $S = 1/2$, Van Vleck (V2) shows that the exchange interaction contributes to the fourth moment but not to the second moment of an absorption line. Since the total area of

the line cannot change, the line will be peaked and the extra area distributed in the wings. This is exchange narrowing.

For dissimilar ions, such as ions precessing about different axes, the exchange interaction tends to bring the two different transitions together and hence produce one wider line. In other words, the exchange interaction contributes to the second moment and we have exchange broadening. In general, both exchange broadening and exchange narrowing are present and the resultant line width depends on the relative contribution of each.

The effect of exchange interaction is well exemplified in the test samples. Copper sulphate shows exchange broadening as a result of the coalescence of the two lines due to the two dissimilar Cu^{2+} ions in the unit cell (B1). For DPPH free radicals, considerable exchange narrowing results in a very narrow line width even in a polycrystalline sample (H2).

2.3 Effect of Crystalline Field

As indicated in section 2.1.2, a paramagnetic ion in a crystal is subjected to a strong inhomogeneous electric field called the crystalline electric field. This field originates in the environment of the paramagnetic ion and consists of (a) static and (b) fluctuating components. The latter is due to the thermal vibration of the lattice and contributes only to the line width (see section 2.2.1). The static component, to the first approximation, will have the same symmetry as the crystal structure. Its effect is to cause a Stark splitting of the energy levels of the ions thereby removing some of the (2J+1) degeneracy.

(J=L+S). The degree to which this degeneracy is lifted depends on the symmetry of the field.

Experimental data reveals that the strength of the various crystalline fields fall into three groups.

(i) In the weak field case, L and S are not uncoupled but still precess around the resultant J which in turn precesses about the direction of the applied electric field. Good examples are the rare earth salts where the unpaired 4f electrons are somewhat shielded from the direct influence of the crystalline field.

(ii) Medium Fields. The coupling between L and S is broken so that they precess about the field separately and J is no longer a good quantum number. It is found that the orbital motions are usually quenched. For example the iron group hydrated salts.

(iii) The field may be so strong as to destroy both the LS coupling and the coupling between the angular momenta and spins of the individual electrons. Again the orbital motion is quenched. This is typified by the iron group cyanides.

2.4 The Theoretical Hamiltonian

The Hamiltonian of an ion in a crystal lattice can be written as the sum of a number of interaction terms. The exact solution is usually obtained for the largest term and the contributions of the remaining terms taken into account by perturbation calculations. The various terms are:

(a) The Coulomb interaction of the electrons with the nuclear charge Ze and the mutual repulsion of the electrons. In the

non-relativistic approximation, it is given by

$$W_F = \sum_{k=1}^{N} (P_k^2/2m - Ze^2/r_k) + \sum_{k > j=1}^{N} e^2/r_{kj}$$

where P_k = linear momentum

r_k = radius vector from nucleus to electron.

(b) The magnetic interaction between the electron spin $\vec{s}_k$ with the orbital momentum $\vec{l}_k$.

$$W_{LS} = \sum_{jk} (a_{jk}\vec{l}_j \cdot \vec{s}_k + b_{jk}\vec{l}_j \cdot \vec{l}_k + c_{jk}\vec{s}_j \cdot \vec{s}_k)$$

where a_{jk}, b_{jk}, c_{jk} are constants.

(c) The mutual interaction between the electronic spins

$$W_{SS} = \sum_{jk} \frac{\vec{s}_j \cdot \vec{s}_k}{r_{jk}^3} - \frac{3(\vec{r}_{jk} \cdot \vec{s}_j)(\vec{r}_{jk} \cdot \vec{s}_k)}{r_{jk}^5}$$

(d) The interaction energy due to the nuclear spin I and nuclear quadrupole moment Q.

$$W_N = 2\gamma\beta\beta_N \sum_k \left\{ \frac{(\vec{l}_k - \vec{s}_k) \cdot \vec{I}}{r_k^3} + \frac{3(\vec{r}_k \cdot \vec{s}_k)(\vec{s}_k \cdot \vec{I})}{r_k^5} + \frac{8\pi}{3}\delta(r_k)\vec{s}_k \cdot \vec{I} \right\}$$

$$W_Q = \frac{e^2 Q}{2I(2I-1)} \sum_k \left\{ \frac{I(I+1)}{r_k^3} - \frac{3(\vec{r}_k \cdot \vec{I})^2}{r_k^5} \right\}$$

Here β_N and γ refer to the nuclear magneton and nuclear

gyromagnetic ratio.

(e) The effect of the external magnetic field H which produces the splitting of the electronic levels between which the transitions are observed.

$$W_H = \sum_k \beta \, (1_k + 2s_k) \cdot H$$

(f) The direct interaction of the nucleus with the external field.

$$W_h = -\gamma \beta_N \, H \cdot I$$

(g) The interaction of the crystalline electric field.

$$W_v = -\sum_k eV(x_k, y_k, z_k)$$

where $V(x_k, y_k, z_k)$ is the potential. The general Hamiltonian is therefore given by

$$\mathcal{H} = W_F + W_V + W_{LS} + W_{SS} + W_H + W_N + W_Q + W_h \qquad (2.5)$$

The order of magnitude of these interactions are $W_F \sim 10^5 \ cm^{-1}$, $W_V \sim 10^3 - 10^4 \ cm^{-1}$, $W_{LS} \sim 10^2 - 10^3 \ cm^{-1}$, $W_{SS} \sim cm^{-1}$, $W_H \sim cm^{-1}$, $W_N \sim 10^{-1} - 10^{-3} \ cm^{-1}$, $W_Q \sim 10^{-3} \ cm^{-1}$, and $W_h \sim 10^{-3} \ cm^{-1}$.

If we confine our discussion only to states which are eigenstates of L and S, eqn. (2.5) can be written as a sum involving terms representing electronic interactions and terms representing nuclear interactions.

A perturbation method of calculation has been given by Pryce (P3) in which the operators referring to spin and nuclear variables are treated as non-commuting algebraic quantities. An expression involving the components of S and I is obtained. This is called the 'Spin Hamiltonian' whose first order approximation gives

$$\mathcal{H} = \vec{S} \cdot D \cdot \vec{S} + \beta \vec{H} \cdot g \cdot \vec{S} + \vec{S} \cdot T \cdot \vec{I} + \vec{I} \cdot P \cdot \vec{I} - \gamma \beta_N \vec{H} \cdot \vec{I}$$

$$- \beta^2 \vec{H} \cdot \Lambda \cdot \vec{H} \qquad (2.6)$$

If the crystalline field has axial symmetry about the z-axis,

$$\mathcal{H} = g_{//} \beta H_z S_z + g_\perp \beta (H_x S_x + H_y S_y) + D \left[S_z^2 - \frac{1}{3} S(S + 1) \right]$$

$$+ A S_z I_z + B(S_x I_x + S_y I_y) + P \left[I_z^2 - \frac{1}{3} I(I + 1) \right]$$

$$- g_N \beta_N \vec{H} \cdot \vec{I} - \beta^2 \vec{H} \cdot \Lambda \cdot \vec{H} \qquad (2.7)$$

S here is the effective electronic spin and is determined by equating the multiplicity of the line observed to 2S. The term in D describes how the levels behave in zero magnetic field in the absence of nuclear interaction. $g_{//}$ and $g_\perp$ are the g values when the field is applied parallel and perpendicular to the crystalline electric field axis respectively. A and B measure the splitting of the hyperfine structure. P refers to the quadrupole splitting and is related to Q through $P = 3eQ \left(\frac{\partial^2 V}{\partial z^2} \right) \Big/ 4I(2I - 1)$. The final term $- \beta^2 \vec{H} \cdot \Lambda \cdot \vec{H}$ representing

a constant interaction independent of $\vec{S}$ or $\vec{I}$ is normally very small and can be neglected. The actual energies are then given by the eigenvalues of the new operator $\mathcal{H}$ in the equation $\mathcal{H}\psi = E_0 \psi$ where ψ represents the wave functions of the effective spin states.

CHAPTER III

DESCRIPTIONS OF APPARATUS

3.1 Introduction

The essential elements of a microwave solid state spectrometer are (a) a monochromatic source, preferably of variable frequency,

(b) a cavity (absorption or reflection type),

(c) a variable magnetic field,

and (d) a detector.

In this chapter, the components of the narrow band, single modulation spectrometer are described in detail. Block diagrams will be employed to illustrate the design principles and the actual circuit diagrams are collected together in the appendix. The spectrometer can function from room to helium temperatures.

3.2 The Microwave System

The Block diagram for the microwave setup is shown in Fig. 3. The photograph in Plate I shows the general arrangement of the microwave components.

3.2.1 The Microwave Power Source

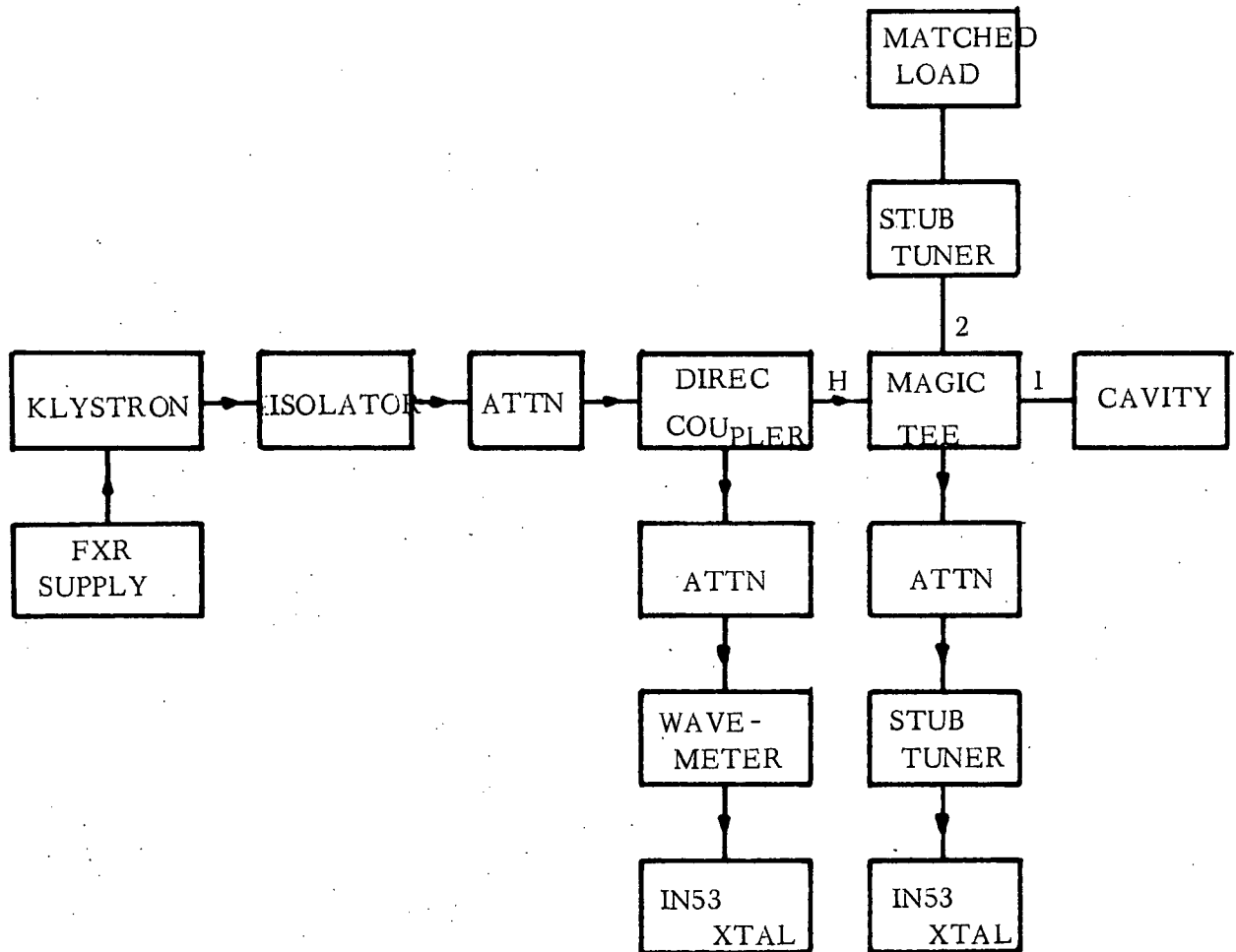Besides having a variable frequency source, a good spectrometer further requires that
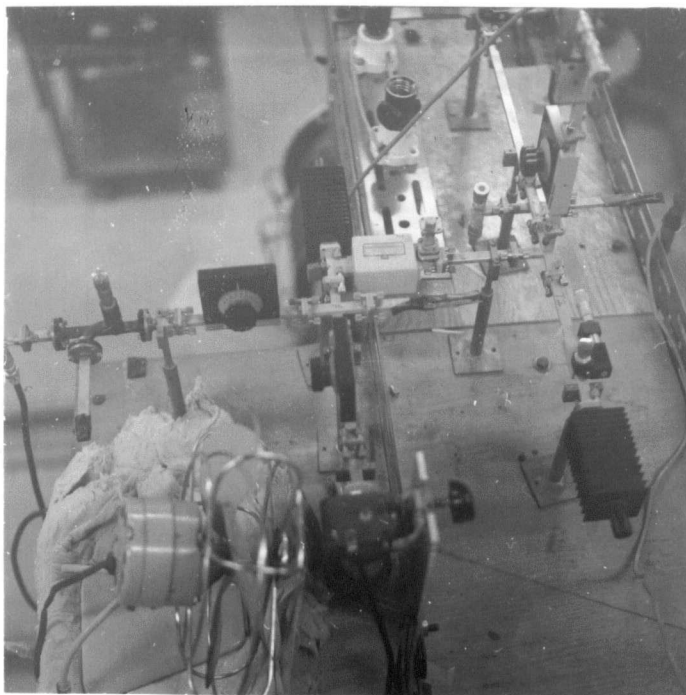
Fig. 3 Block Diagram for 8mm Microwave Circuit.
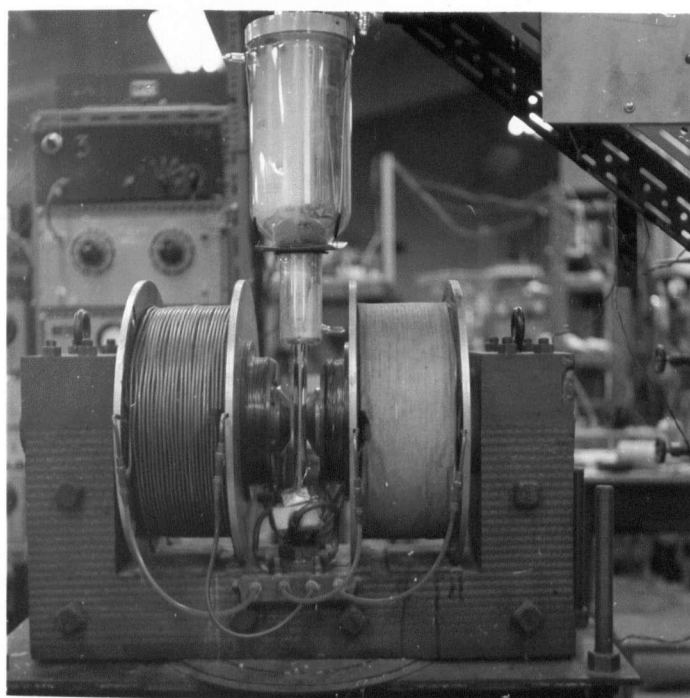
PLATE I   VIEW OF MAIN MICROWAVE ARRANGEMENT

PLATE II   VIEW OF THE MAGNET AND THE CRYOSTAT

(a) the frequency and power be sufficiently stable,

(b) there must be enough power output (usually of the order of
milliwatts),and

(c) a low noise level is desirable for good resolution and
sensitivity.

In the present experiment an EMI valve type reflex klystron (VX5023T)
capable of generating about 50 mW of power is used. This klystron is
tunable from 34.6 to 36.4 Gc/s and is forced air-cooled.

In order to satisfy (a), it is necessary to have a stable low
ripple power supply. We have chosen an FXR Model Z815B Universal
Klystron Power Supply Unit with a regulation of better than 0.3%. The
rms ripple voltage is less than 3 mV for the beam voltage and less than
1 mV on the reflector. Saw-tooth, square-wave, sine wave and pulse
modulations are available at various voltage levels and frequencies.
In the experiment, only saw-tooth modulation was used to sweep through
the klystron reflector mode.

3.2.2 Wave-Guide Components

All of the wave-guide components are commercial units manufactured
by the DeMornay Bonardi Corporation except for the circulator which is
a Cascade Research product. This unit is used to isolate the microwave
source from the rest of the system (G2).

3.2.3 Crystal Detectors

For the detection and monitoring of the microwave power 1N53
silicon diodes are used. These are designed for a centre frequency of
35.0 Gc/s and are mounted on broad-band crystal mounts.

3.2.4 The Cavity Resonator

A circular cylindrical cavity resonator operating in the H_{111} mode has been designed from data given by Wilson (W2). It is made of brass. The choice of the fundamental mode of excitation has the advantage of concentrating the microwave energy at the bottom of the cavity where the sample can be conveniently placed. Care has been taken to choose a size as large as possible within the limitation of the magnet gap such that no interference modes nor crossing modes can exist. This latter precaution reduces the trouble of determining the mode of excitation in the cavity which is very troublesome at 8 mm and below. The cavity used is a fixed size one. However, it is relatively simple to convert to a tunable cavity by incorporating a choke plunger as the termination. The Q of the cavity is of the order of 2000 at room temperature and the diameter and thickness of the coupling hole are respectively 1.5 and 0.2 mm.

3.2.5 Wavelength Measurement

A broadband absorption type low Q cavity frequency meter is employed as an estimate of the klystron frequency by monitoring the power from a directional coupler (Fig. 3). It is a Sperry product and is suitable for operation in the range of 26.5 - 39.0 Gc/s. The absolute accuracy is about 0.1%. This low Q wavemeter is convenient for a rapid estimate of the frequency of the klystron. For more precise work, a high Q wavemeter should be included.

3.3 Magnetic Field Equipment

3.3.1 The Magnet

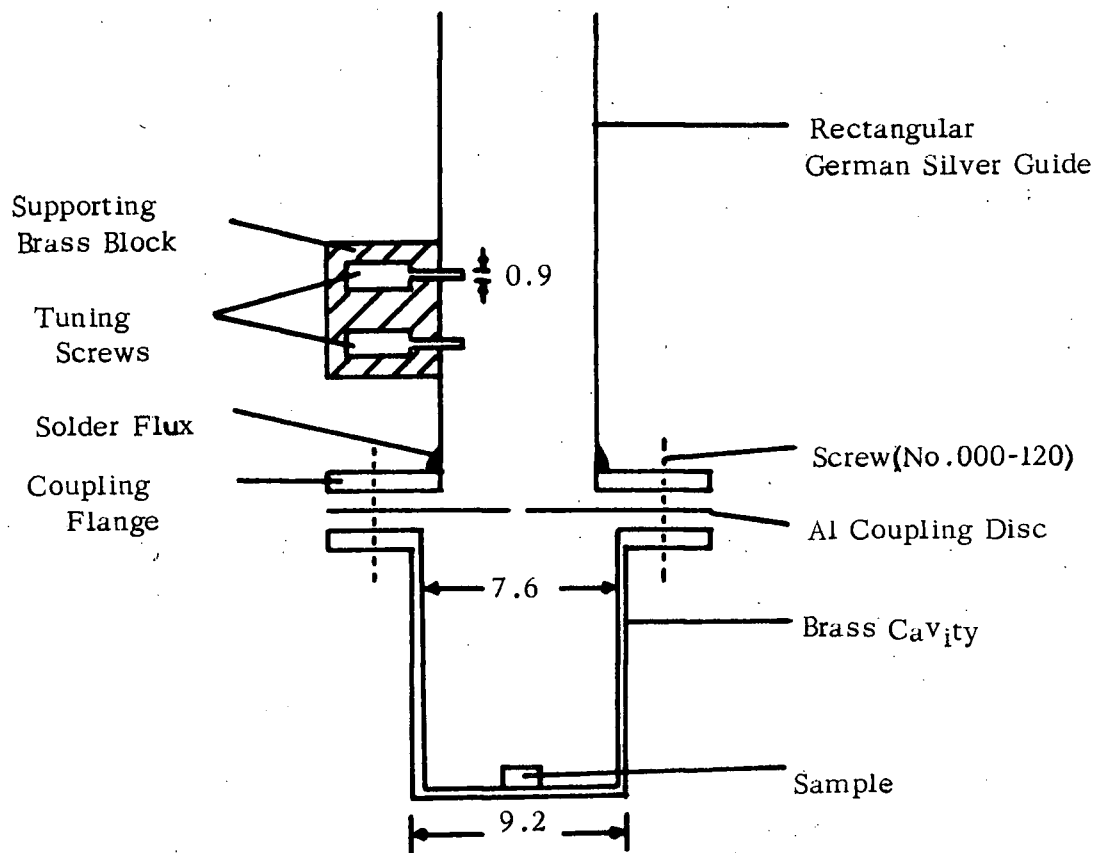A magnetic field intensity of over 10 kilogauss is produced by

Fig. 4 Cross-section of the Cavity.
(All Dimensions in mm.)

a small electromagnet designed by Buckmaster and partly constructed in

the departmental machine shop. For fuller details, reference should

be made to H. A. Buckmaster's thesis (B6). Briefly, the main features

are (a) adjustable gap up to 3"

(b) rotatable magnet yoke (360° with 0.5° calibration)

(c) vertical level adjustment

(d) water cooled

(e) good homogeneity of the order of 0.5%

(f) trolley mounting for ease of moving.

Plate II shows the view of the magnet with the cryostat.

3.3.2 The Magnet Power Supply

The magnet current of up to 15 amperes is supplied by 51 twin-triode

tubes (6AS7G) connected in parallel. The grids are biased to near

cut-off with a regulated power supply (see Appendix). The normal plate

voltage used is 220 volts. This is obtained by connecting two generators

in series since each generator in the Physics Building can give only

150 volts maximum.

The stability thus produced has been measured to be of the order

of $< 0.5\%$. This was done by comparing the voltage developed across

a standard manganin resistor (0.124 ohm) with a standard mercury cell

and the difference detected by a Honeywell null indicator. The field

stability should be much higher since the magnet is working near

saturation. Signal from DPPH have been recorded indicating that the

stability approximates to 1 in 10^4. Such stability is sufficient

for most applications. However, it must be emphasized that higher

stability is required for narrower lines than that of DPPH

($\sim$ 4 gauss).   With the use of transistors, it becomes relatively

inexpensive to build a supply having stability of the order of 1 in 10^5 or better (Gl).

3.3.3 Low Frequency Modulation

A sinusoidal current source is used to drive a pair of Helmholtz coils for low frequency field modulation. The modulator consists of a 6AU6A driver tube whose grid input is fed from an audio-oscillator (Beckman/Shasta Model 301A) and the output is used to control the current flowing through 14 6AS7-tubes all connected in parallel (Appendix). By this means, a large modulation can be obtained.

For the study of narrow lines such as DPPH signals some difficulty arises in the production of small modulation because of the great number of turns of wire (350 turns) in the Helmholtz coils. A convenient solution is to shunt the coils with a variable load. In our case, a 3.2 ohm rheostat is used which can be disconnected whenever a large modulation is needed.

3.4 The Detection System

A three stage, low noise, variable gain amplifier (2.10^6 maximum) of standard design is used to amplify signals from the crystal detector. The design data has been taken from an RCA Receiving Tube Manual (Tech. Series RC-19, 1959). A typical noise level is about $2\,\mu V$ input. The filaments are d.c. heated to reduce hum and the plate voltage is obtained from a regulated Lambda-power supply. It is found that 60 c/s pickup exists despite the precautions taken including the use of coaxial cables between stages.

Following the high gain amplifier is a filter-amplifier to reduce

noise. This is a low gain device and employs a twin-filter with a bandwidth of 20 c/s and centre frequency 135 c/s (V1). In this way it is possible to eliminate 60 cps pickup completely.

Before passing on to a pen-recorder for a permanent record, the amplified signal is fed into a phase sensitive detector. The design follows very closely the one due to Schuster (S1). Normally a bandwidth of 1 or 2 c/s is employed and the recorded signal is the differential of the absorption line.
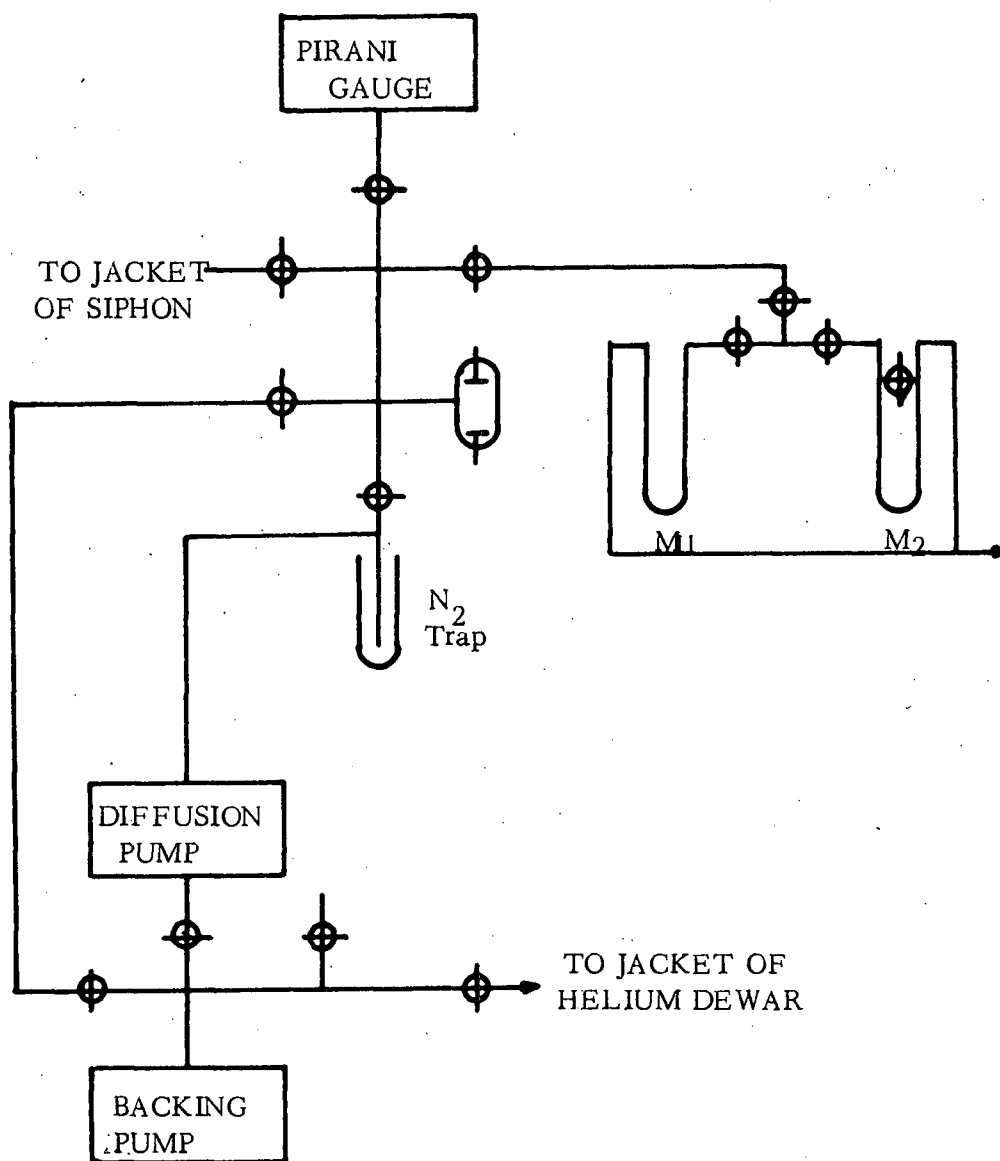
Detailed circuits of all the electronic instruments can be found in the Appendix.

3.5 The Vacuum System

Experimental techniques at low temperatures are well known (W1). In this section, only a brief description will be given.

A schematic representation of the vacuum installation is shown in Fig. 6. M_1 and M_2 are the mercury and oil manometers for measuring pressure in the dewar. The Cenco Supervac oil diffusion pump used is for high speed evacuation down to about a micron of mercury pressure. This is preceded by a backing pump (Cenco Pressovac) capable of producing about 10 microns of pressure. The backing pump, besides pumping down one arm of the manometer, is also used to evacuate the jackets of the transfer syphon and that of the helium dewar.

Fig. 7 depicts a double dewar cryostat arranged concentrically so that the outer forms a liquid nitrogen space surrounding the inner dewar which contains liquid helium. The dewars are made of pyrex glass and silvered by Brashear's chemical method (S2) such that two narrow strips

Fig. 6. A Schematic Diagram of the Vacuum System.

PIRANI
GAUGE

TO JACKET
OF SIPHON

N_2
Trap

M_1 M_2

DIFFUSION
PUMP

TO JACKET OF
HELIUM DEWAR

BACKING
PUMP

M_1 : Mercury Manometer
M_2 : Oil Manometer

To Kinney Pump

V_1

V_2 V_3

Transfer Siphon
inlet

Mica Window
To Waveguide System

To Manometer

Helium Gas Return

Brass Cap

Rubber Sleeve

To Backing pump

Inner Dewar

German   Silver Guide
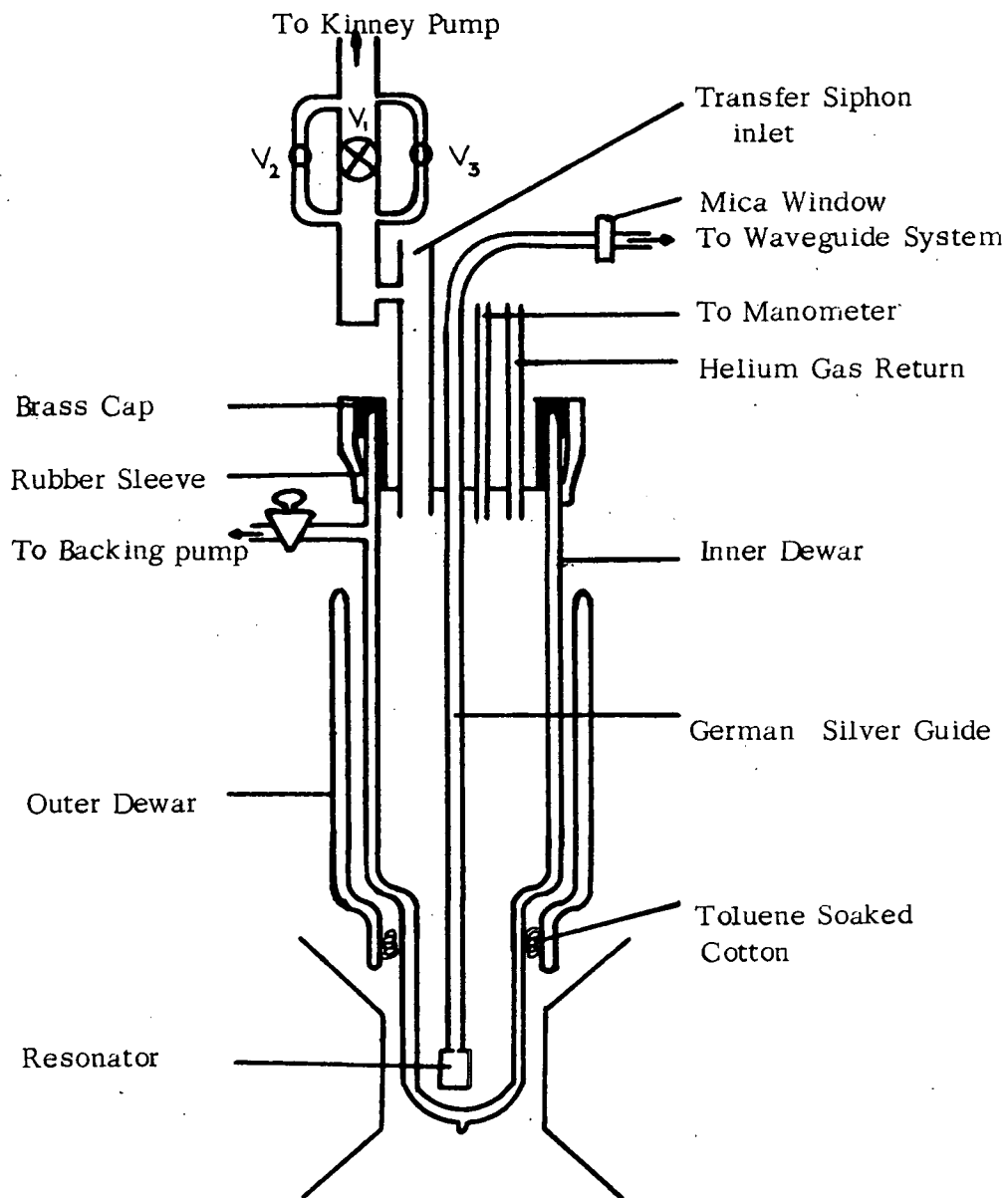
Outer Dewar

Toluene Soaked
Cotton

Resonator

Fig. 7 The Cryostat (Cap Diam. 2.56")

are left for liquid level observation. The helium dewar encloses the
german-silver waveguide terminated by a Q-band resonator. It is topped
with a brass cap (2.56" O.D.) that carries also outlets for the helium
transfer syphon, the manometers, the helium gas return line and the
Kinney pump for pumping over the liquid helium to obtain temperatures
below 4.2^O K. The big control valve V_1 is bypassed by two progressively
smaller valves V_2 and V_3 to allow fine control of the pumping speed.
The lowest temperature normally obtained in this laboratory is about
1.5^O K. A rubber sleeve over the cap and the dewar completes the vacuum
tight compartment. The whole assembly of cap and vacuum system is
mounted rigidly on a Dexion stand.

As a result of the small magnet gap available for experiments, it
has been necessary to make an open-bottomed outer dewar. Cooling of the
lower parts of the helium dewar is then achieved by a continuous stream
of liquid nitrogen flowing over its surface. This method of cooling was
later found to be insufficient and wasteful. A normal helium run lasted
only 2 to 3 hours. In the experiment to be described in chapter 4, the
Kinney pump is not employed as it is uneconomical to lower the temperature
below 4.2^O K.

CHAPTER IV

EXPERIMENTAL PROCEDURE

An outline of a typical paramagnetic resonance experiment at 4.2° K will be given. The procedure for room temperature performance is the same except for the low temperature technique which is then of no concern.

A known amount of the sample under investigation is mounted on the bottom of the cavity with nail varnish (colourless type). Care must be taken to use an amount that will not overload the cavity. The cavity resonator is then properly tightened to the german-silver guide and the klystron power supply switched on together with the fan which cools the klystron valve. Saw-tooth modulation is applied on the reflector so that a whole mode can be swept through and displayed on a Tektronix scope 545A whose sweep is synchronized with the modulating frequency. With the reflected power from the cavity displayed on the scope, the klystron is mechanically tuned until a pip appears on the mode.

To distringuish a true cavity resonance peak from peaks caused by reflections, the following tests have been found useful and convenient. By squeezing the german-silver waveguide, the guide wavelength is increased without causing changes in the frequency of the electro-magnetic radiation. Consequently, peaks caused by reflection which is

a function of the guide wavelength will be shifted in position as seen on the screen while the resonant pip is not affected. As the german-silver guide protrudes above the brass cap, this method is applicable at helium temperatures when other means of cross-checking is difficult to achieve. The other test makes use of the effect of temperature, e.g. cooling down the cavity with liquid nitrogen. As the cavity shrinks its resonant frequency increases causing the pip to move across the screen without affecting the peaks from other reflection.

Once the resonance has been found, the tuning screws in front of the coupling hole are adjusted to give a desired coupling condition. In all the experiments performed, the cavity is slightly undercoupled (Y1).

Now the double dewar cryostat is ready for mounting. After having evacuated the inner dewar, clean helium gas from a cylinder is introduced into the dewar at a few centimeters above atmospheric pressure. The over-pressure is maintained throughout the precooling to ensure that the helium gas is not dirtied when it returns to the helium liquefier in the event of a slight leakage in the vacuum system. As mentioned before (3.5) the outer dewar is different from the conventional one. In order to decrease the flow rate, cotton soaked with toluene is used to block part of the flow (see Fig. 7). However this is not very satisfactory because the adjustment is almost impossible once the toluene has solidified. Subsequently, the open end is completely blocked off and liquid nitrogen is allowed to flow down only through three small tubings which can be seen in Plate (II). They may also be partially blocked if necessary.

When the helium gas inside the inner dewar has cooled down to the lowest temperature attainable, the liquid helium transfer can start. The transferring is achieved by applying an over pressure of 4 cm mercury to the helium in the can. The return line must be opened during the transfer and after to allow the evaporated helium gas to return to the gas holder and the jacket of the transfer syphon is evacuated to 50 μ before the transfer. As soon as enough liquid helium has been syphoned over, the pressure on both sides of the syphon is equalized. The helium can is then removed and the syphon blocked. Since the dielectric helium will get into the cavity, it is necessary to retune the cavity as the resonant frequency will be lowered by about 2.4%.

At this stage the magnet is slowly rolled in place and the experiment is ready to begin. It should be mentioned that for maximum stability of operation, the magnet current is left at about 6 amperes for about 2 hours previous to the experiment to allow the magnet and the power supply to reach thermal equilibrium. The high intensity magnetic field is applied at right angle to the microwave magnetic field.

To observe paramagnetic resonance, the klystron modulation is slowly turned down and the reflector voltage adjusted so that the klystron oscillates at the resonant frequency of the cavity at zero modulation. Then a large field modulation is superimposed on the main field and the signal displayed on the screen. The power input to the cavity may be increased to allow visual observation without additional amplification. The stub tuner in arm 2 of the magic Tee (Fig. 3) is carefully adjusted by varying its penetration and position along the guide until a pure absorption mode appears. The depth of penetration

of the tuner has been intentionally increased to cause some microwave

bucking. However, no attempt has been made to find the optimum amount

necessary for high sensitivity performance. Finally the signal is

recorded with a small field modulation by synchronising the rotation

of the motor of the recorder with the magnet current control dial.

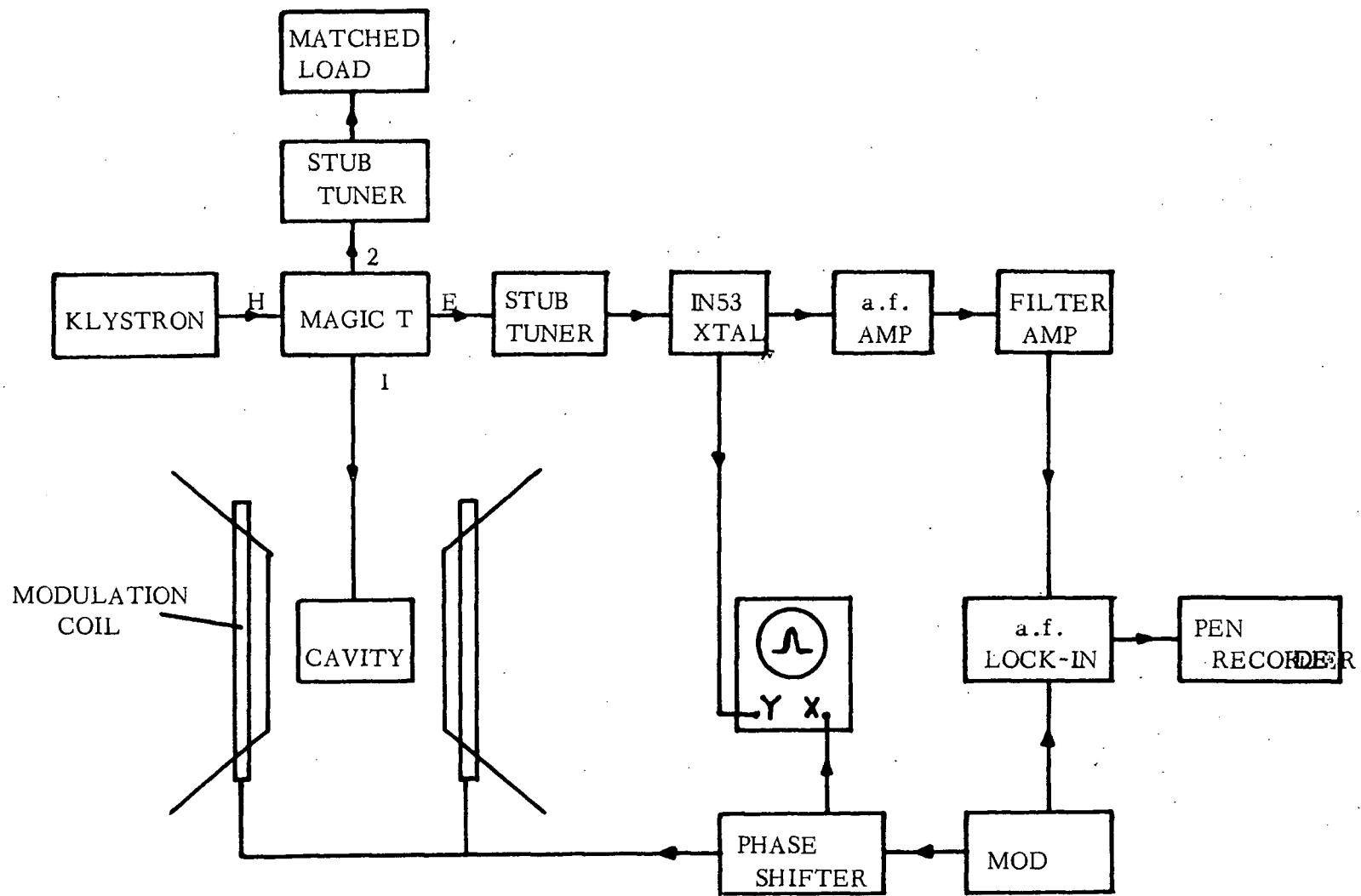The detection scheme is shown in Fig. 5.

Fig. 5 Block Diagram of a Single Modulation Spectrometer.

CHAPTER V

EXPERIMENTAL RESULTS

5.1 Introduction

Electron Spin Resonance (ESR) can be observed with any substance
that has a structure with an unpaired electron (Chapter I). Such sub-
stances are paramagnetic and they include atoms, free radicals,
biradicals, crystals containing paramagnetic ions, crystals with
lattice defects and several other species. However, the phenomenon
of microwave absorption in paramagnetic salts was only first discovered
in 1945 by Zavoisky (Z1), while the paramagnetic resonance of free
radicals was first reported by Holden and others in 1950 (H2, T2). The
experimental technique was greatly advanced by Penrose (P2) in 1949
when he discovered the method of magnetic dilution in order to resolve
the hyperfine structures so often masked by spin-spin interaction.

In this chapter, copper sulphate pentahydrate and DPPH (diphenyl
picryl hydrazyl) are used to test the operation of the spectrometer.
These two substances have often been employed as standards in many ESR
experiments for various reasons. DPPH is a stable free radical that
gives a very strong signal of narrow line width. The copper salt has
been fully studied and analysed both theoretically and experimentally.

5.2 General Information

COPPER SULPHATE PENTAHYDRATE $CuSO_4 \cdot 5H_2O$

The crystal is triclinic, of Space Group C_i^1 and contains two
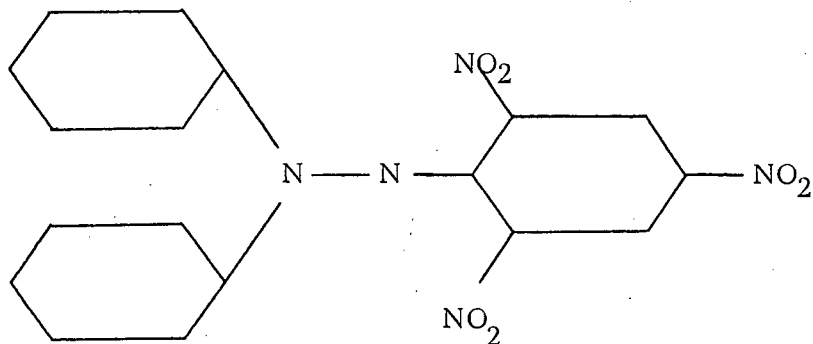
molecules per unit cell (B2).

Unit Cell Dimensions

$$a_0 = 6.12 \text{ Å} \qquad \alpha = 82° 16'$$

$$b_0 = 10.7 \qquad \beta = 107° 26'$$

$$c_0 = 5.97 \qquad \gamma = 102° 40'$$

The axial ratio is a : b : c = 0.5715 = 1 = 0.5575. Measurements

made by Krishnan and Mookherji (K3, K4) showed that it is magnetically

anisotropic. As pointed out by them, the asymmetry of the crystalline

field acting on the paramagnetic ion is the ultimate cause. The most

complete paramagnetic resonance work was due to Bagguley and Griffiths

(B1) who found that the line width varies greatly for different

orientations of the crystal and at different wavelengths used. At

0.85 cm, the line width at room temperature may vary from 25 to 450

gauss. According to our measurement, the line width also seems to

increase at low temperature.

1,1-DIPHENYL-2-PICRYL HYDRAZYL (DPPH)

The stable crystalline DPPH was the first free radical studied by

ESR (H2, T2). Its structural formula is

Subsequently, more detail studies have been done by Hutchison et al (H3) and Kikuchi et al (K1). Since each molecule has one unpaired election associated with it, a very intense signal is obtained. The g-value is slightly anisotropic being in the range of 2.0035 to 2.0041 depending on orientation. For a polycrystalline sample, a half-width of 3.7 Oe is observed at 3 cm wavelength (H3). However, the half-width is only 1.8 gauss when the external field is 3 gauss. Although no special attention has been paid to the measurement of line width, our value is about 5 gauss indicating a possibility of further broadening under higher field intensity.

5.3 Results

The signals obtained from 2.0 mg of $CuSO_4 \cdot 5H_2O$ crystal are shown in Fig. 8. The crystal was mounted on its a^* face with the b-axis approximately at right angle to the static magnetic field. The experiment was carried out at room temperature as well as at 4.2^O K
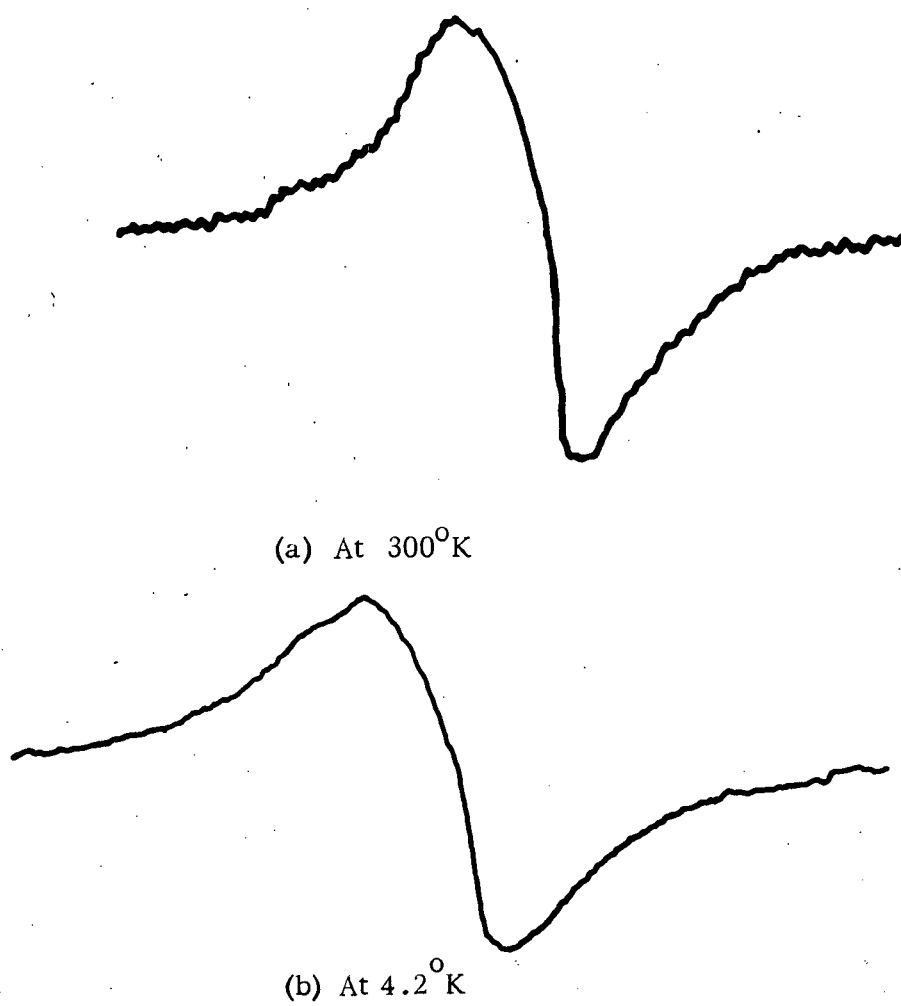
(a) At 300°K

(b) At 4.2°K

Fig. 8 Signals From 2mg of $CuSO_4.5H_2O$ Single Crystal

Fig. 9 Signal From 0.2mg of Powder DPPH

and the modulating field used in each case is about one-fifth of the line width value.

Figure 9 shows the signal from 0.2 mg of DPPH in polycrystalline form. In this case the modulating field is about 0.7 gauss as measured by the voltage induced in a coil located at the centre of the magnet gap.

The sensitivity deduced from these measurements is shown in Table 1. The relevant data for calculation being power input $P_O \sim 1$ mW, bandwidth $\Delta \nu = 1$ cps, unloaded cavity $Q_O = 3000$, noise figure $F = 1$, filling factor $\eta = 1$, line width $\Delta H = 150$, 400, and 4 gauss. Theoretical sensitivities have been calculated using the equation (2.8) (F1).

Mass sensitivity
$$M_{min} = F^{\frac{1}{2}} \ \frac{1}{\pi \ \eta \ Q_O} \ \frac{kT}{\mu^2} \left(\frac{kT \ \Delta \nu}{2P_O} \right)^{\frac{1}{2}} \frac{\Delta H}{H} \frac{M_W}{N_O} \tag{2.8}$$

where F = total noise factor of the detector system

μ = electronic magnetic moment

M_W = molecular weight of the sample

N_O = Avogadro's number

k = Boltzmann's constant

T = temperature in ^{O}K.

TABLE 1

SENSITIVITY OF Q-BAND SPECTROMETER OBTAINED

Sample	Temperature	Ultimate Sensitivity	Experimental Sensitivity
$CuSO_4 \cdot 5H_2O$	300° K	$7 \cdot 10^{-10}$ gm	$2 \cdot 10^{-4}$ gm
	4.2° K	$3 \cdot 10^{-13}$ gm	$4 \cdot 10^{-6}$ gm
DPPH	300° K	$2 \cdot 10^{-11}$ gm	$4 \cdot 10^{-6}$ gm

It seems that the experimental sensitivity is far from satisfying. However, it must be mentioned that the actual filling factor was calculated to be 0.004, 250 times less than the ideal one. Also, the noise figure that can be normally achieved is not 1, but of the order 10. Therefore, the present sensitivity could be easily improved by a hundred fold by increasing the filling factor alone. Further improvement could be achieved by reducing the noise level of the system which is reckoned to be a bit high although the true value was not determined.

For comparison, we give the sensitivity of various spectrometers that have been specially designed for high sensitivity operation. These are shown in Table 2 for the testing sample DPPH only.

TABLE 2

COMPARISON OF SENSITIVITY OF DIFFERENT SPECTROMETERS AT 290° K

Type	Operating Band	Sensitivity	Reference
Single field modulation	X band	3×10^{-8} gm	P1
Super heterodyne detection	X "	8×10^{-9} gm	H1
Single field modulation	K "	8×10^{-9} gm	B6
Double field modulation	K "	1×10^{-11} gm	B7
Single field modulation	Q "	$\sim 10^{-8}$ gm	

CHAPTER VI

CONCLUSION AND DISCUSSION

An 8 mm solid state spectrometer has been tested and found satisfactory in most respects. Although the sensitivity still falls short of the theoretically predicted value, it is comparable to the most sensitive spectrometers reported. The discrepancy probably lies in the fact that the external interferences have not been totally eliminated. The external interferences may be electrical or mechanical in nature. They cause instabilities of about five to ten times the level of random noise (H1). Frequency instability is not a limiting factor as the Q of the cavity is only a few thousand. Electrical interference has been eliminated. Mechanical interference coming from building vibrations has not been taken care of although rather straight-forward shock mounting should eliminate them.

The sensitivity can be increased by improved methods of detection. Using double field modulation, an improvement of about 1000 should be possible as has been demonstrated by Buckmaster (B7). However it may not be an easy task to overcome the problems involved in high frequency modulation since we are now working at a shorter wavelength.

The method of superheterodyne detection applied to the present setup should theoretically give 10^9 times better sensitivity than a

crystal or bolometer detector (M1). This is mainly because of the greatly reduced crystal noise which is inversely proportional to frequency (T1). Under practical conditions, only 5-10 times improvement has been achieved (F1). Moreover, the need for an auxiliary oscillator and an automatic frequency control system to keep the frequency difference between the two oscillators constant makes the superheterodyne more complicated. The auxiliary oscillator may in itself be a further source of noise.
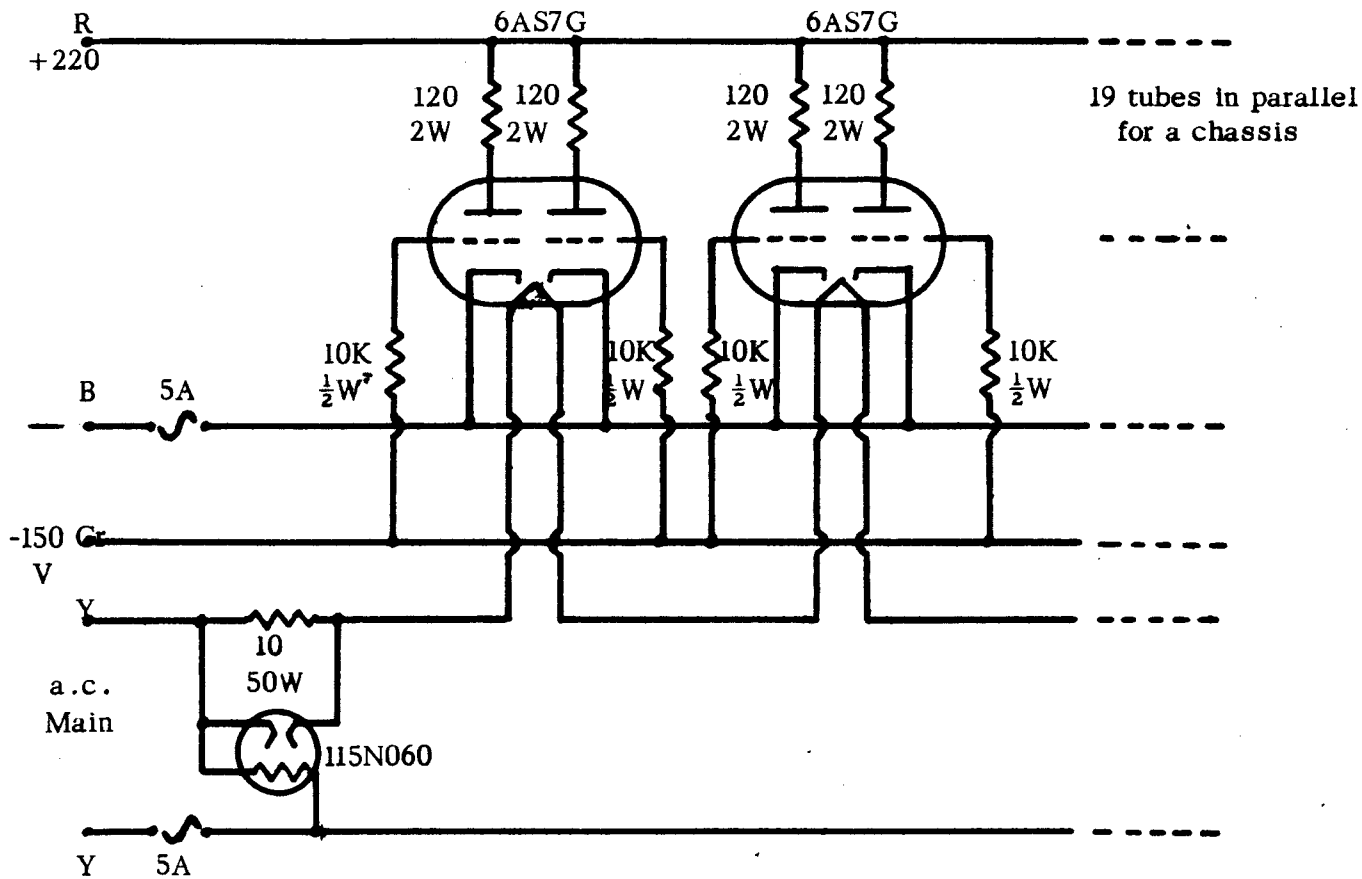
High frequency modulation is not very satisfactory because the increased modulation frequency introduces more pickup originating from the magnetic forces of the static field interacting with the eddy currents induced in the cavity walls by the a.c. field component. With sufficient effort, such as the use of nonconducting walls with plated interior surfaces, it may be possible to reduce the eddy currents (L1).

The best approach, if ultimate sensitivity is not absolutely necessary, seems to be the use of bolometer. The only change needed then is to decrease the modulation frequency since bolometer functions better below 100 cps. Also the problem incurred in designing new detecting instruments will be relatively simple and quickly achieved.
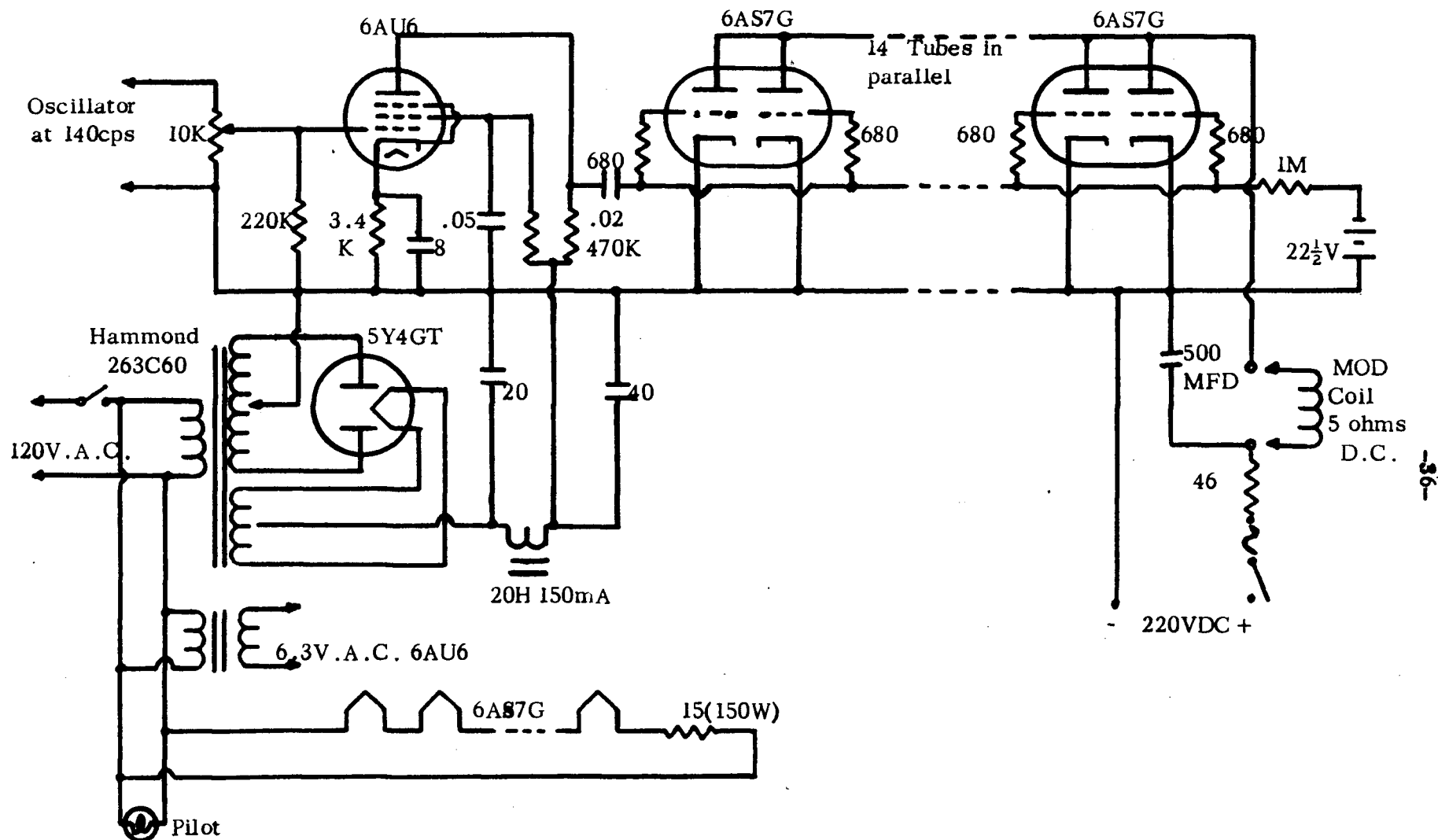
APPENDIX

The circuit diagrams used are collected together in this Appendix. Unless otherwise stated the values for the resistors are in ohms and the capacitors in microfarads.
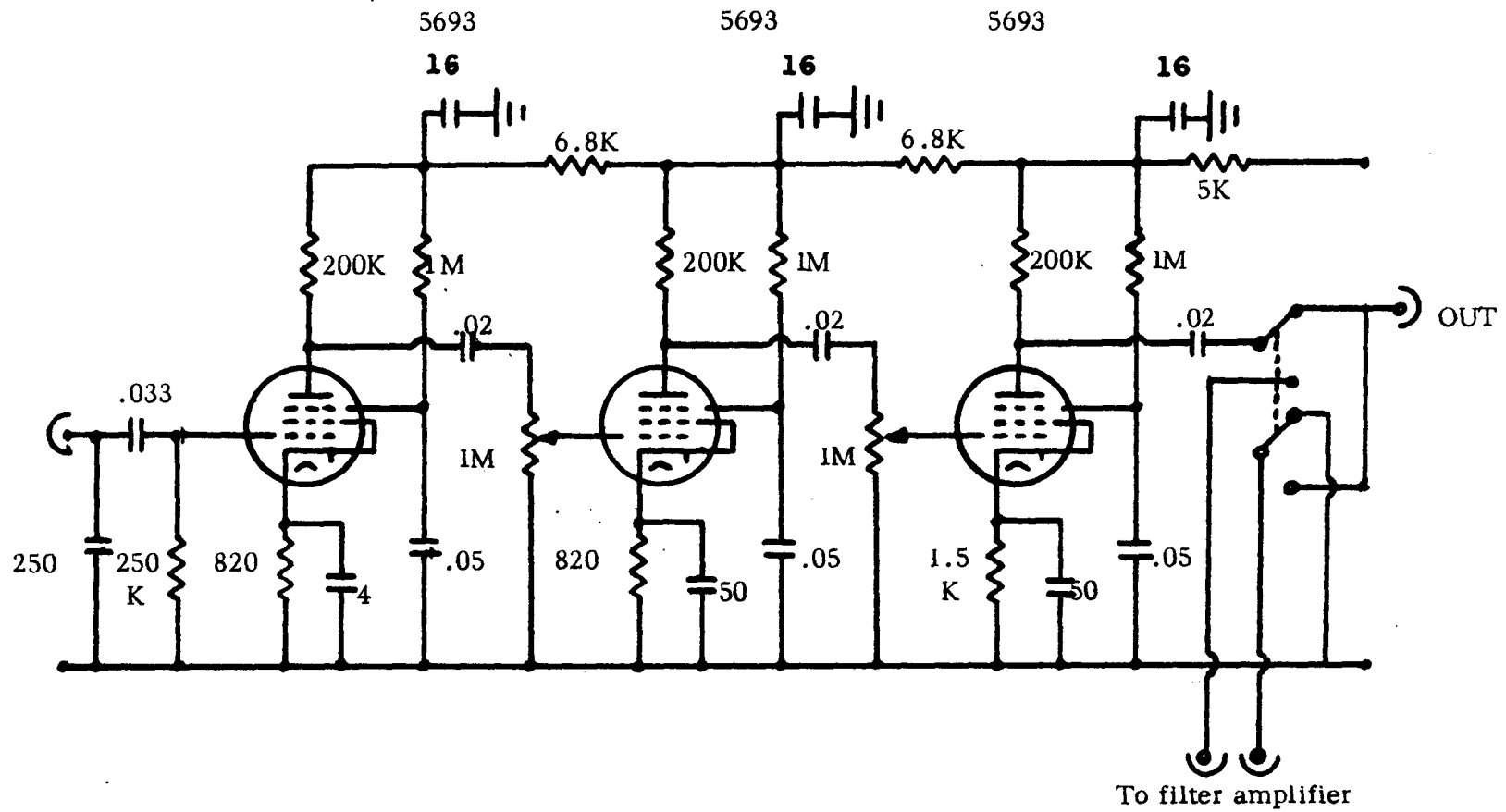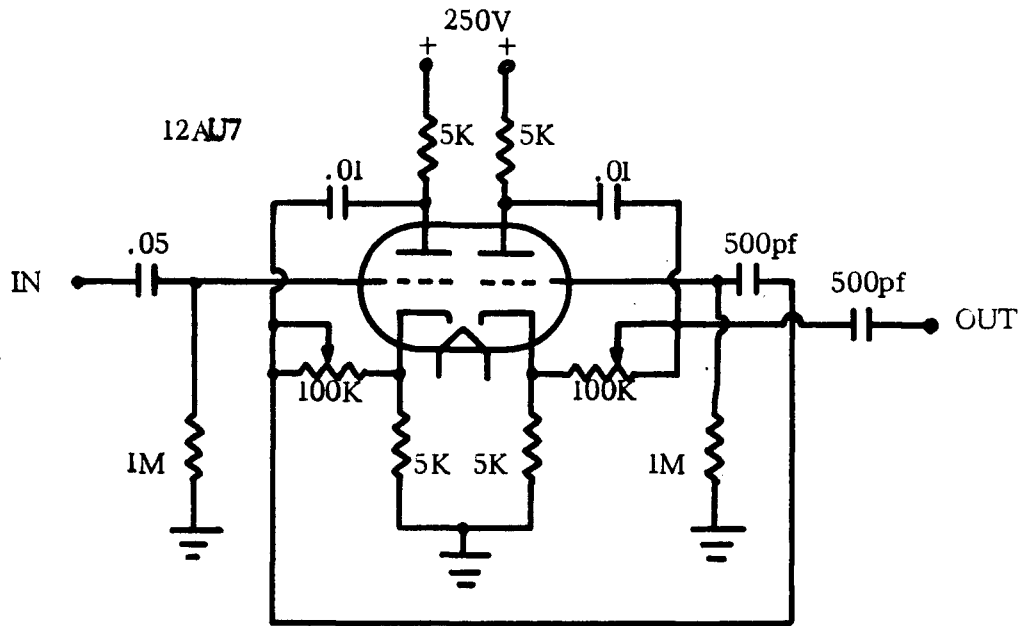
All Resistors "Ohmite"

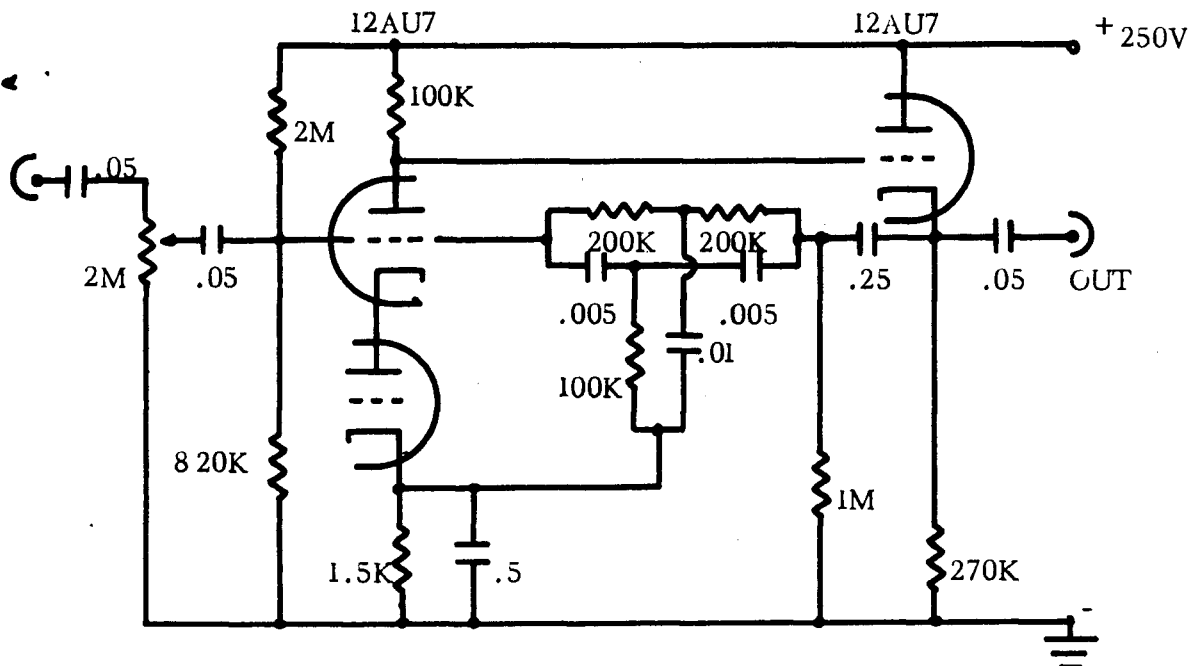Circuit 1. Magnet Current Supply (3 chassis in series).

Circuit 2. Modulation Supply.
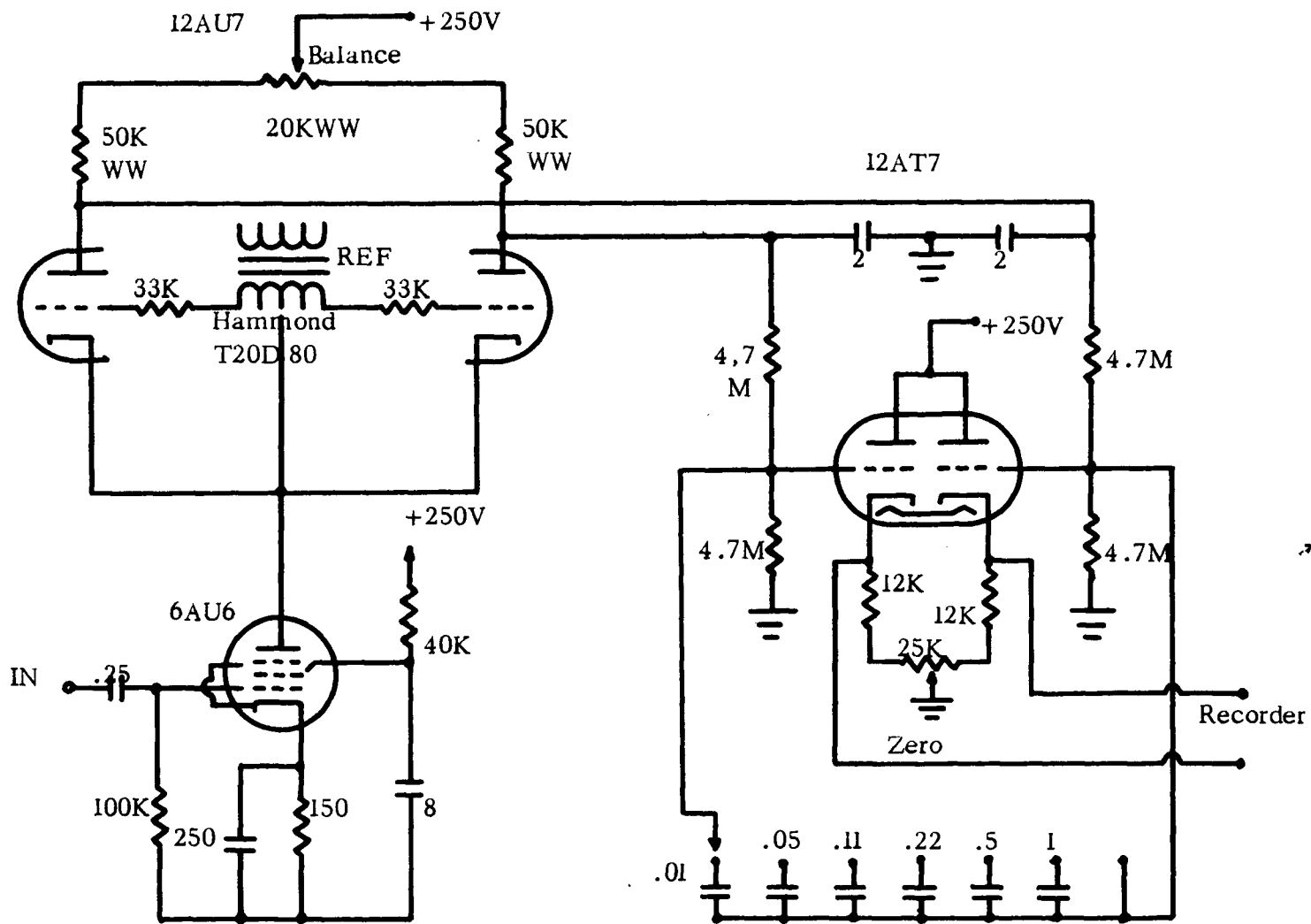
Circuit 3. High Gain Audio Amplifier.

Circuit 4. Phase Shifter.

Values for Twin-Filter are 1%
All Others 10% and $\frac{1}{2}$W

Circuit 5. Filter-Amplifier.

Circuit 6. Phase Sensitive Detector.

BIBLIOGRAPHY

B1   Bagguley, D.M.S. and Griffiths, J.H.E., Proc. Roy. Soc. A201 (1950) 366.

B2   Beevers, C.A. and Lipson, H., Proc. Roy. Soc. A146 (1934) 570.

B3   Bethe, H.A., Ann. Phys., Lpz. 3 (1929) 133.

B4   Bleaney, B. and Stevens, K.W.H., Rept. Prog. Phys. 16 (1953) 108.

B5   Bowers, K.D. and Owen, J., Rept. Prog. Phys. 18 (1955) 304.

B6   Buckmaster, H.A., Ph.D. Thesis, University of British Columbia (1955).

B7   Buckmaster, H.A. and Scovil, H.E.D., Can. J. Phys. 34 (1956) 711.

F1   Feher, G., Bell Syst. Tech. J. 36 (1957) 449.

G1   Garwin, R.L., Rev. Sci. Instr. 29 (1958) 223.

G2   Ginzton, E.L., "Microwave Measurements" (McGraw-Hill, New York, Toronto and London, 1957).

H1   Hirshow, J.M. and Fraenkel, G.K., Rev. Sci. Instr. 26 (1955) 34.

H2   Holden, A., Kittel, C., Merritt, F.R. and Yager, W.A., Phys. Rev. 77 (1950) 147L.

H3   Hutchison, C.A. Jr., Pastor, R.C. and Kowalsky, A.G., J. Chem. Phys. 20 (1952) 534L.

I1   Ingram, D.J.E. "Spectroscopy at Radio and Microwave Frequencies" (Butterworths, London, 1955).

K1   Kikuchi, C. and Cohen, V.W., Phys. Rev. 93 (1954) 394.

K2   Kramers, H.A., Proc. Acad. Sci. Amst. 33 (1930) 959.

K3   Krishnan, K.S. and Mookherji, A., Phys. Rev. 50 (1936) 860.

K4   Krishnan, K.S. and Mookherji, A., Phys. Rev. 54 (1938) 533.

L1   Lambe, J., Ager, R., Rev. Sci. Instr. 30 (1959) 599N.

L2   Low, W., "Paramagnetic Resonance in Solids" Supp. 2, Solid State
     Physics Series (Academic Press, New York and London, 1960).

M1   Misra, H., Rev. Sci. Instr. 29 (1958) 590.

O1   Orbach, R., Proc. Roy. Soc. 264A (1961) 458.

P1   Pake, G.E., Weissman, S.I. and Townsend, J., Disc. Faraday Soc.
     19 (1955) 147.

P2   Penrose, R.P., Nature Lond. 163 (1949) 992.

P3   Pryce, M.H.L., Proc. Phys. Soc. A63 (1950) 25.

P4   Pryce, M.H.L., and Stevens, K.W.H., Proc. Phys. Soc. A63 (1950) 36.

S1   Schuster, N.A., Rev. Sci. Instr. 22 (1951) 254.

S2   Strong, J., Neher, H.V., Whitford, A.E., Cartwright, C.H. and
     Hayward, R., "Procedures in Experimental Physics" 22nd printing
     (Prentice Hall, New Jersey, 1961).

T1   Torrey, H.C. and Whitmer, C.A., "Crystal Rectifiers" (McGraw-Hill,
     MIT Radiation Lab. Series, Vol. 15, p. 187, 1948).

T2   Townes, C.H. and Turkevich, J., Phys. Rev. 77 (1950) 148.

V1   Valley, G.E. and Wallman, H., "Vacuum Tube Amplifiers",
     MIT Radiation Lab. Series, Vol. 18 (McGraw-Hill, New York, Toronto
     and London, 1948).

V2   Van Vleck, Phys. Rev. 74 (1948) 1168.

W1   White, G.K., "Experimental Techniques in Low-Temperature Physics",
     (Clarendon Press, Oxford, 1959).

W2   Wilson, I.G., Schramm, C.W. and Kinzer, J.P., Bell Syst. Tech. J.
     25 (1946) 408.

Y1   Yariv, A. and Clapp, F., Rev. Sci. Instr. 30 (1959) 684.
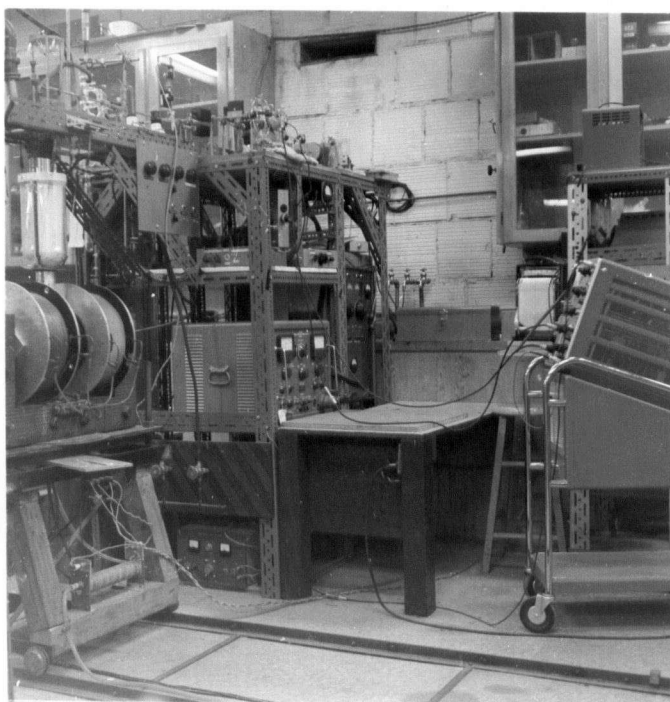
Z1   Zavoisky, E., J. Phys. USSR 9 (211) 1945.

PLATE III   GENERAL VIEW OF THE APPARATUS